Available online at www.sciencedirect.com

SCIENCE DIRECT

Thin Solid Films 492 (2005) 180 – 186

www.elsevier.com/locate/tsf

Effect of germanium addition on the properties of reactively sputtered ZrN films

D. Pilloud [a], J.F. Pierson [a,*], A. Cavaleiro [b], M.C. Marco de Lucas [c]

[a] *Département CREST, Institut FEMTO-ST (UMR CNRS 6174), Université de Franche-Comté, Pôle Universitaire, BP 71427, 25211 Montbéliard cedex, France*
[b] *Departamento de Engenharia Mecânica, Universidade de Coimbra, Polo II, ICEMS, FCTUC, Pinhal de Marrocos, 3030 Coimbra, Portugal*
[c] *Laboratoire de Recherches sur la Réactivité des Solides (UMR CNRS 5613), Université de Bourgogne, 9 Av. Alain Savary, BP 47870, 21078 Dijon cedex, France*

Received 16 December 2004; received in revised form 13 June 2005; accepted 22 June 2005
Available online 26 July 2005

Abstract

For the first time, Zr–Ge–N films were deposited on silicon and steel substrates by sputtering a Zr–Ge composite target in reactive Ar–N_2 mixture. The films were characterised by electron probe microanalysis, X-ray diffraction, micro-Raman spectroscopy and depth-sensing indentation. The effects of the Ge content and substrate bias voltage on the films' structure, internal stress, hardness and oxidation resistance were investigated. Substrate bias strongly influenced the chemical composition of the films being observed by means of a steep decrease in the Ge content for negative bias voltages higher than −80 V. In these cases, a significant hardness improvement was registered. For −100 V biased films, in the Ge concentrations range tested in this study, only ZrN grains were evidenced by X-ray diffraction. The film compressive stresses increased with the germanium concentration. An unexpected effect of the Ge content on the films' hardness was observed. In spite of the increase in the compressive stresses of the films with increasing Ge content, the hardness monotonously dropped from 38 GPa for pure ZrN down to 21.5 GPa for 4.6 at.% Ge. Addition of Ge into ZrN-based coatings induced an improvement of the oxidation resistance and it favoured the tetragonal form of zirconia in oxidised Zr–Ge–N coatings.

Keywords: Reactive sputtering; ZrN; Hardness; Oxidation

1. Introduction

Transition metal nitrides coatings are widely used as diffusion barriers in microelectronics, hard wear-resistant coatings on cutting tools or as corrosion- and abrasion-resistant layers on optical and mechanical components [1]. Among the different transition metal nitrides (TiN, CrN, HfN, TaN, etc.) zirconium nitride is an attractive material due to its good chemical and physical properties. Although ZrN exhibits a slightly higher oxidation resistance than TiN, it is also sensitive to air oxidation at temperature as low as 600 °C [2,3]. To improve the oxidation resistance and/or the mechanical properties of zirconium nitride coatings, several elements have already been added: Al [4], C [5], Ce [6], Cu [7], Ni [8], Si [9], Ti [10], Y [11] etc. To the best of the author's knowledge, there is no paper related to the effect of germanium addition on the properties of zirconium nitride coatings. Moreover, only little information is available in the literature concerning the effect of germanium addition on the properties of transition metal nitrides thin films. In previous papers, it was reported that hard Zr–Si–N films can be deposited by reactive sputtering a Zr–Si composite target [12] and that the oxidation resistance of ZrN films in the 600–750 °C range was improved by silicon addition [13]. Using the same deposition procedure, Zr–Ge–N coatings have been developed. The choice of germanium as doping element of ZrN films can be justified by the relative similar behaviour of silicon and germanium (atomic radius, ability to form a nitride, immiscibility with

* Corresponding author. Tel.: +33 3 81 99 46 72; fax: +33 3 81 99 46 73.
E-mail address: jean-francois.pierson@pu-pm.univ-fcomte.fr (J.F. Pierson).

0040-6090/$ - see front matter © 2005 Elsevier B.V. All rights reserved.
doi:10.1016/j.tsf.2005.06.051

ZrN, etc.) and by the lowest price of Ge chips compared to that of Si. Thus, the aim of this work is to investigate the effect of the addition of germanium in low contents on the ZrN coating properties (structure, internal stress, hardness and oxidation resistance).

2. Experimental details

Zr–Ge–N films were deposited on silicon (100) and polished X38CrMoV5 steel substrates by DC magnetron sputtering a 200-mm-diameter Zr–Ge composite target in $Ar–N_2$ reactive mixture. The deposition system (Alcatel SCM 650) was equipped with a load lock chamber for quick and convenient substrates exchange. Before the introduction of the substrates in the deposition chamber, they were cleaned in acetone and ethanol. The substrate holder was connected to a radiofrequency generator (13.56 MHz). Prior to the deposition, the substrates were cleaned by argon sputter etching during 15 min using a bias voltage of −230 V. During the last 5 min, the target was simultaneously sputtered in $Ar–N_2$ mixture. To avoid the substrate contamination during the target cleaning, a shield was interposed between the substrates and the target. In this study, the following deposition conditions were kept constant: the substrate-target distance (60 mm), the regulated intensity applied to the target (1.5 A), the nitrogen flow rate (5 sccm) and the argon flow rate (5 sccm). Then, the total pressure was close to 0.3 Pa. Zr–Ge–N coatings were deposited without external heating. Thus, the deposition temperature was expected to be close to 150 °C. The germanium concentration in the deposited films was adjusted by the variation of the number of Ge chips ($10 \times 10 \times 1$ mm^3) located on the target erosion zone. In this part of the study, the bias voltage was fixed at −100 V. The effect of the bias voltage on the films' properties was also investigated by varying the bias voltage between 0 and −120 V (the number of Ge chips located on the target was kept at 8).

The films' thickness was measured by profilometry (Dektak 3030) and their chemical composition was determined by a Cameca SX50 electron probe microanalysis (EPMA). The films structure was studied by X-ray diffraction (XRD) using a X'PERT MPD Philips diffractometer with Cu K_α radiation in $\theta/2\theta$ mode or in small angle incidence (0.7°). The crystallite size was estimated from the full-width at half-maximum of X-ray diffraction line using the Scherrer formula, neglecting peak broadening due to residual stresses of the films. The internal stress in the deposited films (σ) was estimated by the curvature (R) of a silicon substrate using the Stoney's formula:

$$\sigma = \frac{1}{6}\frac{E_s}{1-v_s}\frac{t_s^2}{t_f}\frac{1}{R} \quad (1)$$

where: E_s is the substrate Young's modulus, v_s denotes the substrate Poisson's ratio (for Si (100), $E_s/(1-v_s)=180.5$ GPa), t_s and t_f correspond to the substrate and to the film thickness, respectively (in this study, $t_f=1$ μm). It is worthwhile noting that only stress measurements were performed using 1-μm-thick films; other analyses were performed using 3-μm-thick films deposited on steel substrates. This resulted from the relatively low adherence of 3-μm-thick Zr–Ge–N films on silicon substrates. The hardness of about 3-μm-thick films deposited on steel substrates was measured by depth-sensing indentation using a Fischerscope H100 apparatus with a Vickers indenter and a 35 mN applied load.

Oxidation tests of about 3-μm-thick films deposited on steel substrates were performed in air using a conventional furnace at 700 °C during 2 h. The heating rate from room temperature to the annealing one was fixed at 250 °C h^{-1}. After oxidation, the films were analysed by X-ray diffraction in $\theta/2\theta$ mode to study the structural evolution of the remaining Zr–Ge–N film and in small angle incidence to study the nature of the oxide layer. Micro-Raman spectroscopy was also used to characterise the nature of the oxide layer. The apparatus was a Jobin-Yvon T64000. The 514.5-nm line of an Ar^+ laser was used as excitation source.

3. Results and discussion

3.1. Effect of the bias voltage

Among the different deposition parameters that can affect the properties of reactively sputtered films; the bias voltage is one of the most efficient. Then, the effect of the bias voltage on the films' structure, composition and hardness has been studied. The influence of the bias voltage applied to the substrate holder during the films' growth on the X-ray diffractogram is depicted in Fig. 1. In the range from −80 V to 0 V, the deposited films only show a broad peak placed at $2\theta \sim 33°$ with low intensity, suggesting, without TEM

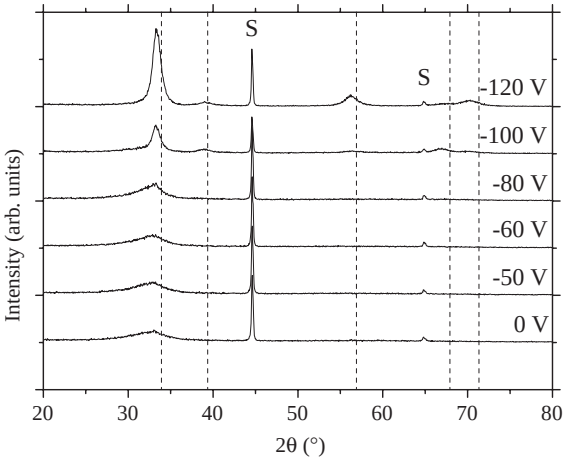

Fig. 1. Evolution of X-ray diffraction patterns vs. the bias voltage. Vertical dot lines and S labels are related to the position of ZrN and substrate diffraction peaks, respectively.

analysis, an amorphous-like structure. For higher negative bias voltage, ZrN crystals are evidenced by XRD. This structural modification has to be correlated with the chemical composition evolution of the films (Fig. 2). Unbiased Zr–Ge–N coating contains a high amount of germanium (approximately 13 at.%). Compared to Zr–Si–N films [12], this germanium concentration is consistent with the amorphous-like state of the deposited Zr–Ge–N coatings. When the negative bias voltage increases, a decrease of the germanium concentration is observed. Up to −80 V, the germanium content is still higher than 7 at.%. For higher negative substrate bias values, the Ge concentration drops abruptly to about 1 and 0.1 at.% when the voltage is −100 and −120 V, respectively. These results clearly show that a strong preferential resputtering of germanium atoms occurred during the films' growth. In summary, at low Ge content, only ZrN grains are evidenced by XRD while at high Ge content (>7 at.% in this study), Zr–Ge–N films show an amorphous-like structure. The Ge content and the structural changes of Zr–Ge–N films deposited with substrate bias also influence the films' hardness as presented in Fig. 2. Independently of their Ge content, amorphous-like Zr–Ge–N films exhibit a constant hardness of 17.5±0.5 GPa. This value is close to that reported for amorphous Zr–Si–N films [12,14,15], indicating that in amorphous-like Zr–X–N films (X=Si or Ge), the hardness seems to be independent of the Si or Ge concentration. On the other hand, crystallised Zr–Ge–N films with Ge concentration lower than about 1 at.% exhibit a hardness higher than 30 GPa. These results clearly show that in Zr–X–N films, the hardness is strongly dependent on the films' structure (crystallised or amorphous-like) and on the X content in crystallised films.

3.2. Effect of the germanium concentration

The evolution of X-ray diffractograms of Zr–Ge–N films as a function of the germanium concentration in the 0–4.6 at.% range is displayed in Fig. 3. Whatever the germanium content, only the fcc ZrN phase is detected by

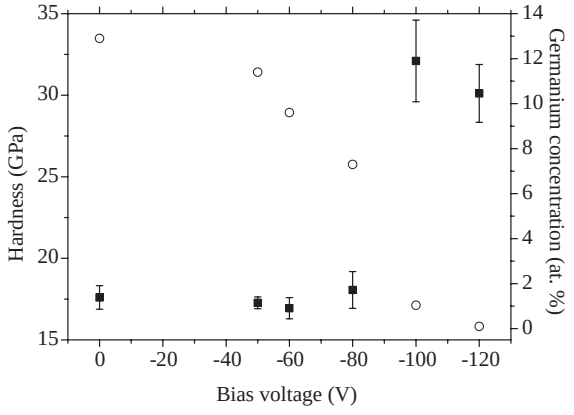

Fig. 2. Effect of the substrate bias voltage on the films hardness (full squares) and the germanium composition (open circles).

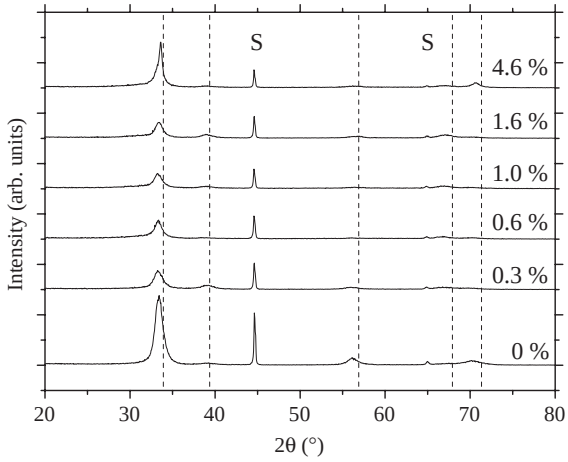

Fig. 3. Influence of the germanium content (in at.%) on the X-ray diffraction patterns of the films. Vertical dot lines and S labels are related to the position of ZrN and substrate diffraction peaks, respectively.

X-ray diffraction. No diffraction peak of germanium-containing compound has been observed on Zr–Ge–N films. As previously published [16], ZrN films grow with a [111] preferred orientation. Contrary to Zr–Si–N films [12], the incorporation of Ge into ZrN-based films does not change the films' texture. Indeed, the Zr–Ge–N coatings also grow with a [111] preferred orientation. At low germanium content (<2 at.%), the grain size estimated from the full-width at half-maximum of the ZrN (111) diffraction peak varies in the 7–9-nm range, independently of the germanium concentration. On the other hand, the film containing 4.6 at.% Ge exhibits a higher grain size—about 13 nm. Furthermore, the diffractogram of this film also shows an unsymmetrical (111) ZrN peak that can be deconvolved into two components: the first one fits well with the (111) ZrN diffraction peak and the second one corresponds to a broad peak as a shoulder at low angles indicating low-order degree, probably an amorphous-like phase. It is worthwhile noting that for the other germanium contents, this shoulder is hardly observed.

Incorporation of germanium into ZrN-based coatings induces a strong modification of the internal stresses of the films (Fig. 4). Indeed, "pure" ZrN coatings exhibit internal compressive stresses close to 2.3 GPa resulting from the ion bombardment during the films' growth when the −100 V bias voltage is applied to the substrate holder [16]. At low germanium content (<2 at.%), the films' compressive internal stresses increase linearly with the germanium concentration up to 3.6 GPa. This strong increase of the stresses may be explained by considering the incorporation of germanium atoms into the ZrN lattice as previously reported for Zr–Si–N films [12]. According to the atomic radius of N, Ge and Zr, germanium atoms may be dissolved in the ZrN lattice in interstitial positions. In fact, due to the lower atomic radius of Ge in comparison to Zr, its inclusion in substitution of Zr positions could not induce compressive stresses. When the germanium content exceeds its solubility

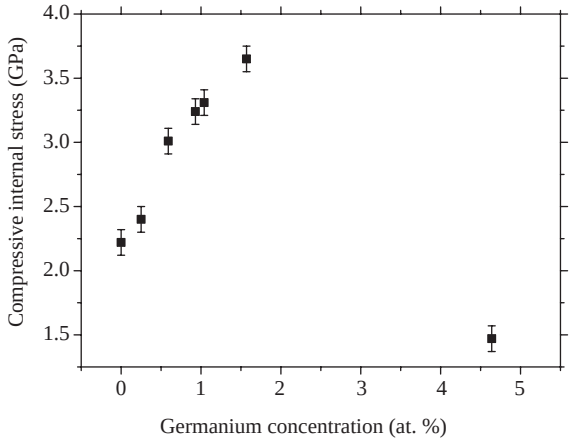

Fig. 4. Variation of the films internal stress vs. the germanium concentration.

limit into ZrN, Ge atoms may be segregated resulting in a decrease of the films' compressive stress to 1.5 GPa for 4.6 at.% Ge. This behaviour is very close to that reported for Zr–Si–N films synthesised in the same deposition conditions and within the same reactor [12].

The preserving of the [111] texture of Zr–Ge–N films, the strong increase of their compressive stresses and the segregation of germanium atoms when the solubility limit is exceeded should induce an increase of the Zr–Ge–N films hardness as commonly observed in Ti–Si–N films [17–20]. Despite these favourable three points, a surprising hardness drop is observed when the germanium content increases (Fig. 5). ZrN films exhibit hardness close to 38 GPa. Incorporation of germanium at concentration as low as 1.6 at.% induces a hardness decrease down to 28 GPa while the films compressive stresses increase by a factor close to 1.6. Before trying to speculate about this contradictory result, several possible reasons for the hardness decrease were eliminated. The first was related to the films thickness. It was confirmed that there was not any significant change in the film thickness with increasing Ge contents which eliminates any possible influence of the substrate in the measured hardness values. In all cases, the maximum

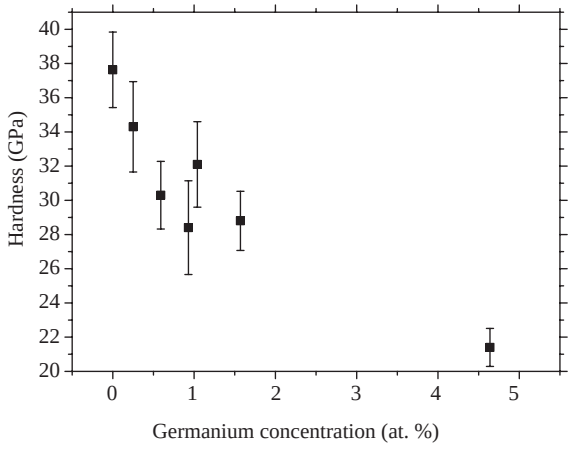

Fig. 5. Effect of the germanium content on the films hardness.

indentation depth over film thickness ratio was always less than 0.1, assuring the exclusive measurement of the film hardness. The second reason could be related to the reliability in the experimental tests. Both hardness and residual stresses measurements were repeated and similar trends were reached, not being observed important changes worthily remarking (the error bars in Figs. 4 and 5 take into account both series of measurements). A tentative explanation for the observed decrease in the hardness with increasing Ge contents can be related to the excess of interstitial atoms in the NaCl-type lattice of ZrN. Andrievski [21] has reported a strong drop in the hardness values for over-stoichiometric Ti–N sputtered films, i.e., for N contents higher than 50 at.%. The suggested reason for that is the increasing number of vacancies in the metal sublattice of the TiN phase as a consequence of the excess of interstitial atoms. In the case of the present study, Ge atoms in interstitial positions can contribute to the increase in the vacancy number since the overall N content in the films as determined by EPMA is higher than 50 at.% (Table 1). The decrease in the hardness originated by this fact will be superimposed to the hardening effect of the higher compressive stress values arising with increasing Ge content, giving rise to an overall drop in the final hardness of the films. For the highest Ge concentration (4.6 at.%), the decrease of the residual compressive stresses led to a further drop in the hardness, the film reaching a value as low as 21.5 GPa.

In spite of the fact that germanium addition into ZrN-based coatings did not lead to improvements in the mechanical properties of the coatings, it will be shown in the next section that, as for silicon, Ge addition improves the films' oxidation resistance.

3.3. Oxidation resistance of Zr–Ge–N films

In a previous paper, the effect of silicon addition on the oxidation resistance of ZrN-based coatings was presented [13]. It was shown that a 3-μm-thick ZrN film is completely oxidised into monoclinic zirconia after a thermal treatment of 2 h at 700 °C. Moreover, the diffraction peaks of iron oxides (α- and γ-Fe_2O_3) evidenced by XRD after oxidation indicated that the substrate was strongly oxidised (no diffraction peak of the ferritic steel was observed). When

Table 1
Chemical composition of Zr–Ge–N films deposited using a −100 V bias voltage

Zr content (at.%)	N content (at.%)	Ge content (at.%)
44.6	55.4	0.0
48.0	51.7	0.3
45.6	53.8	0.6
45.1	53.9	0.9
44.7	54.2	1.0
46.6	51.8	1.6
40.6	54.7	4.6

only small amounts of germanium are added to ZrN-based coatings, improvements on the oxidation resistance can be noticed. Indeed, for oxidation conditions similar to those described above for the ZrN film, the 3-μm-thick Zr–Ge–N film with only 0.3 at.% Ge still shows the diffraction peak of the ferritic substrate, suggesting a lower degree of degradation (Fig. 6). In addition to the unoxidised steel diffraction peak, monoclinic zirconia (m-ZrO_2) and maghemite (γ-Fe_2O_3) peaks are also evidenced. It should be remarked that for undoped ZrN film, only these oxides were detected by XRD, indicating a thicker oxide scale than in Ge-doped film and a lower oxidation resistance. With increasing germanium content, a progressive improvement in the oxidation resistance of the films was reached as suggested by the decreasing intensity of the γ-Fe_2O_3 diffraction peaks down to become undetectable when the germanium concentration exceeds 1.6 at.%.

Besides the oxidation resistance improvement, the germanium addition to ZrN-based coatings induces also a change in the nature of the oxide layer. X-ray diffraction patterns obtained in $\theta/2\theta$ and glancing modes of an oxidised Zr–Ge–N film containing 4.6 at.% Ge are displayed in Fig. 7. In $\theta/2\theta$ mode, m-ZrO_2 is detected with another form of ZrO_2–tetragonal zirconia (t-ZrO_2)–whereas in small angle incidence, only the t-ZrO_2 phase is evidenced. In addition to the occurrence of the t-ZrO_2 phase, XRD analysis also shows that the (111) diffraction peak of ZrN is much narrower than that of the as-deposited film. The mean crystallite size has been estimated to about 21 nm after oxidation compared to 13 nm before (Section 3.2). These results indicate that Zr–Ge–N films exhibit low thermal stability during treatment at 700 °C when compared to Zr–Si–N films with nearly the same Si content [13].

Micro-Raman spectra support the structural change of zirconia vs. the germanium concentration observed by XRD. The spectrum of the film with 0.3 at.% Ge is displayed in Fig. 8a. All the bands detected in the 80–700-cm^{-1} range can be assigned to the monoclinic form of zirconia [22–25]. By contrast, the spectrum of the film with 4.6 at.% Ge (Fig. 8b) displays, in addition to the m-ZrO_2 bands, new bands at about 148, 274, 318 and 463 cm^{-1}. They have been assigned to the tetragonal form of zirconia [24–26]. Then, the oxide layer of the richest Ge film contains both m-ZrO_2 and t-ZrO_2 as observed by XRD in $\theta/2\theta$ mode. Even if pure t-ZrO_2 layer was not formed in the samples with the studied Ge contents, these results indicate that the addition of Ge into ZrN-based coatings tends to stabilise the t-ZrO_2 form. The role of germanium in favouring the tetragonal phase of zirconia during the oxidation of Zr–Ge–N coatings at the expense of the other forms will be discussed later.

Before that, it is worthwhile noting that the experimental positions of the m-ZrO_2 Raman bands in the spectrum of Fig. 8a are slightly shifted with respect to the positions given in the literature for m-ZrO_2 [22–25]. The value and the sign of the shift are different for each Raman band.

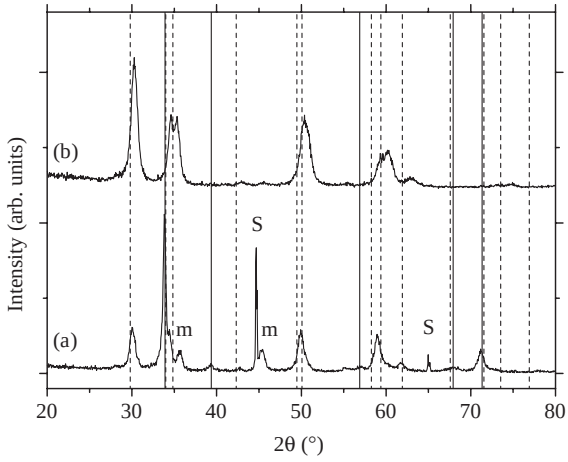

Fig. 7. X-ray diffractogram (a) in $\theta/2\theta$ mode and (b) in small angle incidence (0.7°) of a 4.6 at.% Ge film after oxidation at 700 °C. The vertical solid and dash lines, m and S labels are related to the theoretical position of ZrN, t-ZrO_2, m-ZrO_2 and steel substrate diffraction peaks, respectively.

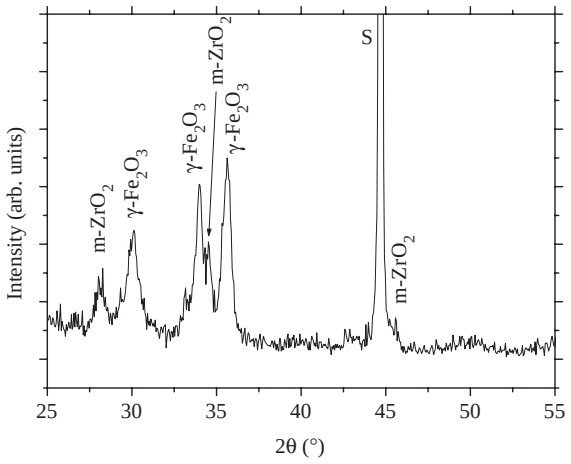

Fig. 6. X-ray diffractogram of oxidised Zr–Ge–N films containing 0.3 at.% Ge. The substrate diffraction peak is located at about 44.6°.

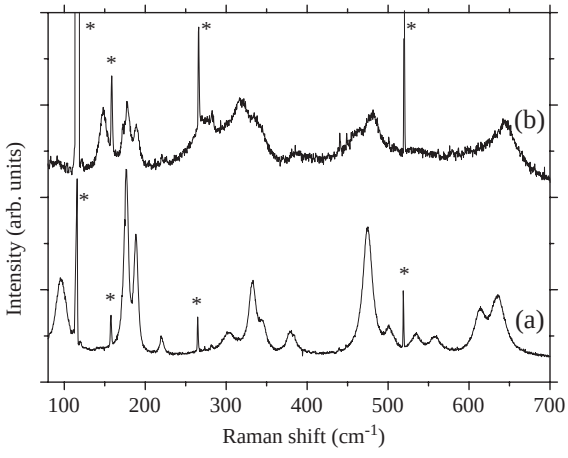

Fig. 8. Raman spectra of Zr–Ge–N films deposited with different germanium contents and oxidised at 700 °C (a) 0.3 at.% and (b) 4.6 at.%. Ar^+ laser plasma lines are labelled by an asterisk (*).

Moreover, the shifts are not observed in all zones of the oxidised surface. The spectrum where the shifts are observed corresponds to regions where the oxidised film remains attached covering large areas of the substrate (Fig. 9b). On the other hand, the positions of Raman bands in the spectrum obtained in isolated scales of areas where extensive spalling of the oxide film occurred during the oxidation process (Fig. 9a) are in good agreement with those reported for m-ZrO_2. For example, the lowest energy band of the m-ZrO_2 spectrum, detected at 97 cm^{-1} in the case of isolated scales, is shifted down to 5 cm^{-1} to lower energies in the spectrum obtained in regions where the oxidised film covers large areas of the substrate. On the contrary, the band recorded at 477 cm^{-1} in the spectrum of isolated scales is shifted up to 5 cm^{-1} to higher energies in large oxidised film areas. Other bands, such as those at 178 and 190 cm^{-1}, are detected almost at the same position independently of the analysed region. These results can be explained by considering the high residual stresses in the oxidised films. In isolated scales, the stresses are relaxed and no shifts occur in relation to standard band positions. The shift in the band position allows to calculate the approximate value of the oxide scale stress. If the Raman shifts were considered to be due to hydrostatic pressures, using the $d\omega/dP$ values reported by Kourouklis and Liarokapis [23] for the 477 cm^{-1} band ($d\omega/dP = -1.4$ cm^{-1}/GPa), the 5 cm^{-1} shift would be related to a stress value of about 4 GPa. This high stress would explain the breakage of the film during the oxidation process.

It is well known that three factors can favor one crystalline structure of zirconia (i.e., monoclinic, tetragonal or cubic) in relation to the other ones: (1) the presence of doping elements, (2) the total pressure involved during the materials formation (i.e., the internal stress) and (3) the grain size. In Zr–Ge–N coatings, the sole element that can create oxygen vacancies in the zirconia network to stabilize t-ZrO_2 during the oxidation process is nitrogen. However, as previously observed in Zr–Si–N [13] or Ti–Si–N coatings [27], this element is not detected in the oxide layer after the oxidation. The occurrence of compressive stresses in the oxide layer is the second factor that can stabilize t-ZrO_2. In Fig. 7, it appears clearly that the diffraction peaks of t-ZrO_2 are shifted to higher values of the diffraction angles in relation to the JCPDS standard values, indicating possible tensile stresses in the oxidised film. Thus, this factor should not be considered to explain the t-ZrO_2 stabilisation. Finally, the third factor that can stabilise t-ZrO_2 is the grain size. In spite of the fact that the monoclinic form is the stable phase of zirconia at room temperature, the tetragonal form can be stabilised when the crystallite size is lower than a critical value, due to the higher surface energy of m-ZrO_2 compared to that of t-ZrO_2 [28]. Meldrum et al. [29] have estimated that the critical grain size is about 12 nm. In the oxidised Zr–Ge–N coating with 4.6 at.% Ge, the t-ZrO_2 mean crystallite size is close to 10 nm, as calculated from the full-width at half-maximum of the (101) t-ZrO_2 diffraction peak. Thus, the stabilisation of the tetragonal zirconia may result from the grain size effect, as previously reported for oxidised Zr–Si–N coatings [13].

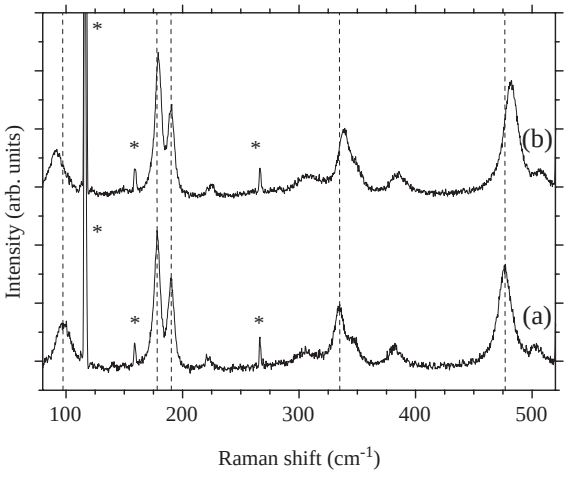

Fig. 9. Raman spectra of oxidised Zr–Ge–N film with 0.3 at.% Ge (a) isolated scales and (b) adherent oxide layer. Vertical dash lines are related to the position of Raman bands in unstressed m-ZrO_2 (i.e., isolated scales). Ar^+ laser plasma lines are labelled by an asterisk (*).

4. Conclusion

Zr–Ge–N films have been deposited on steel and silicon substrates by reactive sputtering of a composite Zr–Ge target. For the first time, the effect of germanium on the properties of ZrN-based coatings has been studied and compared to that previously observed for the silicon-doped films. The effect of the applied bias voltage during the films' growth on the composition and the hardness of Zr–Ge–N coatings has been investigated. It has been shown that germanium atoms are preferentially resputtered with increasing substrate bias voltages. Furthermore, it has been observed that in amorphous-like Zr–Ge–N films, the hardness is independent of the Ge content. The films deposited with −100 V bias voltage are crystalline and presented the highest hardness value.

In the whole Ge concentrations range tested in this study, only ZrN diffraction peaks are evidenced by XRD. Furthermore, addition of Ge into ZrN-based coatings does not modify the ZrN grains' preferred orientation in contrast to Zr–Si–N films. At low Ge content, the films' compressive stresses increase with the germanium concentration which can be explained as due to interstitial incorporation of this element into the ZrN lattice. When the Ge concentration exceeds its solubility limit, Ge atoms may be segregated resulting in a decrease of the compressive stresses. In this study, a very surprising effect of the Ge concentration on the films' hardness has been observed. Indeed, the films' hardness decreases when the Ge content increases, in spite of an increase of the compressive stresses by a factor close to 1.6.

Finally, the oxidation resistance of Zr–Ge–N films during air annealing at 700 °C has been tested. As for Zr–Si–N coatings, addition of Ge to ZrN-based coatings improves the oxidation resistance of the films. In addition to this beneficial effect, it has been shown that germanium stabilises the tetragonal form of zirconia by the grain size effect.

Acknowledgements

This work has been financially supported by CAPM (Communauté d'Agglomération du Pays de Montbéliard), FEDER (Fonds Européen de Développement Régional), AUILF (Action Universitaire Intégrée Luso-Française) and the Conseil Regional de Bourgogne. The LERMPS is acknowledged for its technical support.

References

[1] L. Hultman, Vacuum 57 (2000) 1.
[2] L. Krusin-Elbaum, M. Wittmer, Thin Solid Films 107 (1983) 111.
[3] H.N. Al-Shareef, X. Chen, D.J. Lichtenwalner, A.I. Kingon, Thin Solid Films 280 (1996) 265.
[4] H. Spillmann, P.R. Willmott, M. Morstein, P.J. Uggowitzer, Appl. Phys., A 73 (2001) 441.
[5] M. Morstein, P.R. Willmott, H. Spillmann, M. Döbeli, Appl. Phys., A 75 (2002) 647.
[6] Q.G. Zhou, X.D. Bai, X.Y. Xue, Y.H. Ling, X.W. Chen, J. Xu, D.R. Wang, Appl. Surf. Sci. 226 (2004) 236.
[7] J. Musil, P. Zeman, H. Hrubý, P.H. Mayrhofer, Surf. Coat. Technol. 120/121 (1999) 179.
[8] J. Musil, P. Karvánková, J. Kasl, Surf. Coat. Technol. 139 (2001) 101.
[9] M. Nose, M. Zhou, T. Nagae, T. Mae, M. Yokota, S. Saji, Surf. Coat. Technol. 132 (2000) 163.
[10] L.A. Donohue, J. Cawley, J.S. Brooks, Surf. Coat. Technol. 72 (1995) 128.
[11] Q.G. Zhou, X.D. Bai, X.Y. Xue, Y.H. Ling, X.W. Chen, J. Xu, D.R. Wang, Vacuum 76 (2004) 517.
[12] D. Pilloud, J.F. Pierson, A.P. Marques, A. Cavaleiro, Surf. Coat. Technol. 180/181 (2004) 352.
[13] D. Pilloud, J.F. Pierson, M.C. Marco de Lucas, M. Alnot, Appl. Surf. Sci. 229 (2004) 132.
[14] T. Mae, M. Nose, M. Zhou, T. Nagae, K. Shimamura, Surf. Coat. Technol. 142/144 (2001) 954.
[15] M. Nose, W.A. Chiou, M. Zhou, T. Mae, M. Meshii, J. Vac. Sci. Technol., A, Vac. Surf. Films 20 (2002) 823.
[16] D. Pilloud, A.S. Dehlinger, J.F. Pierson, A. Roman, L. Pichon, Surf. Coat. Technol. 174/175 (2003) 338.
[17] F. Vaz, L. Rebouta, P. Goudeau, J. Pacaud, H. Garem, J.P. Rivière, A. Cavaleiro, E. Alves, Surf. Coat. Technol. 133/134 (2000) 307.
[18] S.H. Kim, J.K. Kim, K.H. Kim, Thin Solid Films 420/421 (2002) 360.
[19] P.J. Martin, A. Bendavid, Surf. Coat. Technol. 163/164 (2003) 245.
[20] M. Nose, Y. Deguchi, T. Mae, E. Hondo, T. Nagae, K. Nogi, Surf. Coat. Technol. 174/175 (2003) 261.
[21] R.A. Andrievski, J. Mater. Sci. 32 (1997) 4463.
[22] B.K. Kim, H.O. Hamaguchi, Phys. Status Solidi, B Basic. Res. 203 (1997) 557.
[23] G.K. Kourouklis, E. Liarokapis, J. Am. Ceram. Soc. 74 (1991) 520.
[24] B. Alzyab, C.H. Perry, R.P. Ingel, J. Am. Ceram. Soc. 70 (1987) 760.
[25] J.E. Maslar, W.S. Hurst, W.J. Bowers Jr., J.H. Hendricks, J. Nucl. Mater. 298 (2001) 239.
[26] E. Djurado, P. Bouvier, G. Lucazeau, J. Solid State Chem. 199 (2000) 399.
[27] M. Diserens, J. Patscheider, F. Lévy, Surf. Coat. Technol. 120/121 (1999) 58.
[28] R.C. Garvie, J. Phys. Chem. 69 (1965) 1238.
[29] A. Meldrum, L.A. Boatner, R.C. Ewing, Nucl. Instrum. Methods Phys. Res., B Beam Interact. Mater. Atoms 207 (2003) 28.